

Phosphorescent Platinum Dyads with Cyclometalated Ligands: Synthesis, Characterization, and Photophysical Studies[†]

Biwu Ma,[‡] Peter I. Djurovich, Muhammed Yousufuddin, Robert Bau, and Mark E. Thompson*

Department of Chemistry and Department of Chemical Engineering and Materials Science, University of Southern California, Los Angeles, California 90089-0744

Received: January 21, 2008; Revised Manuscript Received: March 4, 2008

The synthesis, characterization, and photophysical properties are reported for a series of (C[^]N)Pt dyad complexes with cyclometalated ligands (C[^]N: *F* = 2-(4',6'-difluorophenyl)pyridyl, tpy = 2-(4'-methylphenyl)pyridyl, thpy = 2-(2-thienyl)pyridyl, and btp = 2-(2-benzothienyl)pyridyl). The dyads are connected with a bridging ligand, sym-tetraacetylene (tae), that consists of two 2,4-pentadionate units covalently linked at the 3-position. Stepwise synthesis was applied to obtain both homoleptic and heteroleptic dyads that have been characterized by ¹H NMR and elemental analysis. X-ray crystallographic analysis shows a near orthogonal orientation of the two diketonate moieties in the di-tpyPt (84°) and FPt-thpyPt (89°). An investigation of the photophysical properties of the dyads has been carried out. For homodyads, the emission characteristics are governed by the nature of the cyclometalating ligand, allowing the emission to be tuned throughout the visible spectrum. The di-FPt and di-tpyPt dyads show a modest decrease in luminescent lifetimes compared to their mononuclear analogs. The di-FPt complex undergoes efficient self-quenching by an excimer that is presumed to have only π – π interactions. The heterodyads exhibit efficient intramolecular triplet energy transfer leading to the luminescence almost exclusively from the lower-energy moiety. The energy transfer is presumed to be mediated through the bridging tae ligand by a Dexter-like mechanism involving a combination of hopping and superexchange processes.

Introduction

The design and synthesis of molecular dyads containing electroactive or photoactive units have attracted significant attention for their applications in fields such as molecular light-energy conversion devices, chemosensors, and molecular electronics.^{1–9} It is also of great interest to understand the fundamental properties involved in the photoinduced energy or electron transfer that occurs in these systems.^{10–12} Numerous studies have been conducted on linked donor–bridge–acceptor dyads containing transition-metal complexes (such as Ru, Os, Rh, Pd, Ir, and Pt) as chromophores and using different kinds of ligands as molecular bridges. It has been found that the nature of the bridging ligands strongly affects the electronic properties because the size, shape, and electronic nature of linkage can control the intermetallic electronic communication in such dyads.^{13–28} The distance dependence of energy transfer has been studied extensively and been found to operate via two mechanisms: Förster transfer,²⁹ which favors long-distance interactions, and Dexter transfer,³⁰ dominant in short-range. A distance of 10 Å is normally regarded as the crossing point between the two mechanisms.³¹ So far, however, few studies have examined short-range triplet energy transfer between different transition-metal chromophores in well-defined geometric relationships. It occurred to us that sym-tetraacetylene (tae), a nonaromatic bridging ligand with two diketonate units set almost perpendicular to one another when coordinated to two metal centers,^{32–34} would permit such an investigation. The orthogonal geometry

of this bridging ligand should exert a pronounced effect on the Förster-type transfer because this process is strongly dependent on the geometric orientation of the interacting transition dipoles.^{11,35} With the proper choice of metal complexes as chromophores, the competing roles played by the Förster and Dexter mechanisms in intramolecular energy transfer could then be elucidated in these bimetallic systems.

Neutral platinum(II) and iridium(III) complexes having a monoanionic ligand (C[^]N) as the cyclometalating ligand and a diketonate such as acetylacetonate (acac) as the ancillary ligand have been studied extensively for their luminescent properties.^{36–39} Many of these complexes have been successfully applied as phosphorescent dopants in the fabrication of highly efficient organic light emitting diodes (OLEDs).⁴⁰ Through variation of the cyclometalated ligands, the excited-state energy of the complexes can be tuned to give different emission colors ranging from blue to green and red, with room-temperature lifetimes in microseconds. The electronic transitions responsible for the luminescence in those complexes have been assigned to a mixture of metal-to-ligand charge transfer (MLCT) and ligand centered charge transfer (π – π^*). Because of their attractive luminescent properties, such as high quantum efficiency and long emissive lifetimes, these complexes are ideal candidates for other fundamental photophysical studies. Therefore, it is not surprising that numerous dyad systems have appeared that incorporate transition-metal complexes with cyclometalated Ir derivatives.^{41–46} An important difference between platinum complexes and iridium complexes is that platinum complexes with one cyclometalating ligand typically have a square-planar configuration, whereas the iridium complexes with two cyclometalating ligands display an octahedral coordination environ-

[†] Part of the "Larry Dalton Festschrift".

* Corresponding author. E-mail: met@usc.edu.

[‡] Current address: Materials Science Division, Lawrence Berkeley National Laboratory, Berkeley, California 94720.

ment. The lower symmetry of the Pt cyclometalates makes them preferable over the Ir analogs for use as photoactive units in the investigation of triplet energy transfer across the geometrically constrained π - π bridging ligand. The presence of only a single chromophoric ligand in the Pt complexes makes it straightforward to establish the dipolar relationships between interacting moieties of the dyad.

Herein, we report the synthesis, characterization, and photophysical studies of a series of dyad complexes that use a π - π ligand to link together two cyclometalated Pt(II) species. Both homo- and heterodyads have been prepared. The homodyads exhibit photophysical properties similar to those of their mononuclear species, that is, the same emission energies with equivalent lifetimes. Highly efficient energy transfer is found in the heterodyads, leading to the luminescence from the Pt cyclometalate with lower triplet energy. The factors that control triplet energy transfer in these dyads can be discerned because of the orthogonal geometry of the dyads, which inhibits transfer that operates by a Förster mechanism. The molecular orbitals that participate in the energy-transfer process are then identified with aid of theoretical calculations.

Experimental Section

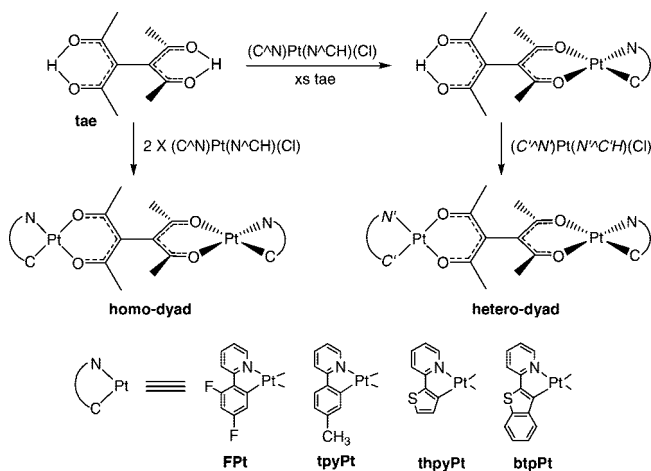
Equipment. The UV–visible spectra were recorded on a Hewlett-Packard 4853 diode array spectrometer. Photoluminescent spectra were measured using a Photon Technology International fluorimeter. Emission lifetime measurements were performed using time-correlated single photon counting on an IBH Fluorocube instrument with excitation provided by a 405 nm pulsed diode laser having a pulse duration of ca. 1.2 ns and an energy of 500 nJ/pulse.

NMR spectra were recorded on Bruker AM 360 MHz instrument. The Microanalysis Laboratory at the University of Illinois, Urbana–Champaign performed all elemental analyses. The program of PhotochemCAD was used to calculate the spectral overlap integrals and Förster radii for intramolecular energy transfer of the heterodyads.⁴⁷

Cyclic voltammetry and differential pulse voltammetry were performed using an EG&G potentiostat/galvanostat model 28. Anhydrous DMF (Aldrich) was used as the solvent under a nitrogen atmosphere, and 0.1 M tetra(*n*-butyl)ammonium hexafluorophosphate was used as the supporting electrolyte. A Pt wire acted as the counter electrode, a Ag wire was used as the pseudo reference electrode, and the working electrode was glassy carbon. The redox potentials are based on values measured from differential pulse voltammetry and are reported relative to an internal ferrocenium/ferrocene ($\text{Cp}_2\text{Fe}^+/\text{Cp}_2\text{Fe}$) reference. Electrochemical reversibility was determined using cyclic voltammetry.

Diffraction data for di-*tpyPt* and *FPt-tpyPt* were collected at room temperature ($T = 23^\circ\text{C}$) on a Bruker SMART APEX CCD diffractometer with graphite-monochromated Mo K radiation ($\lambda = 0.71073 \text{ \AA}$). The cell parameters for the Pt complex were obtained from the least-squares refinement of the spots (from 60 collected frames) using the SMART program. A hemisphere of the crystal data was collected up to a resolution of 0.75 \AA , and the intensity data was processed using the Saint Plus program. All calculations for structure determination were carried out using the SHELXTL package (version 5.1). Initial atomic positions were located by Patterson methods using XS, and the structure was refined by least-squares methods using SHELX with 6983 independent reflections and within the range of $\Phi = 1.38\text{--}24.71^\circ$ (completeness 98.8%). Absorption corrections were applied by using SADABS. Calculated hydrogen

SCHEME 1



positions were input and refined in a riding manner along with the attached carbons.

Synthesis and Characterization. Cyclometalated ligands were prepared following literature procedures as reported previously.³⁹ Other commercial available ligands and materials were purchased from either Aldrich Chemical Co. or Frontier Scientific and used without further purification.

All procedures were carried out in inert gas atmosphere despite the air stability of the complexes, the main concern being the oxidative and thermal stability of intermediates at the high temperatures in the reactions. The Pt(II) chloro-mononuclear complexes were prepared by a modified method of Lewis.^{48,49} This involves heating the K_2PtCl_4 salt with 2–2.5 equiv of cyclometalating ligand in a 3:1 mixture of 2-ethoxyethanol (Aldrich) and water to 80°C for 16 h followed by isolation by filtration after aqueous workup. For syntheses of homoleptic dyads, the chloro-mononuclear complexes were subsequently treated with half-equiv of the bridging ligand and 5 equiv of Na_2CO_3 in dichloromethane and refluxed for 24 h. The yield of homoleptic dyads is 30–40%. For the heteroleptic dyads, the chloro-mononuclear complexes were first treated with 2 equiv of the bridging π - π ligand and 2 equiv of Na_2CO_3 in dichloromethane at room temperature overnight to get mononuclear complexes with a π - π ligand. The mononuclear complexes with

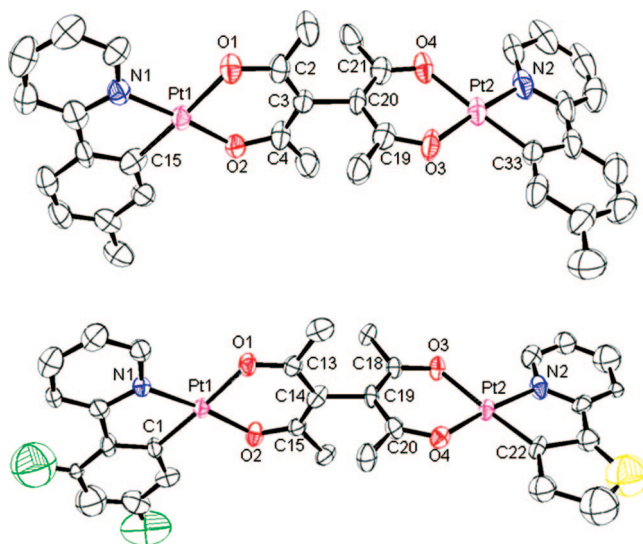


Figure 1. ORTEP diagram of homodyad di-*tpyPt* (top) and heterodyad *FPt-tpyPt* (bottom).

TABLE 1: Selected Bond Lengths and Angles for Di-tpyPt and FPt-thpyPt

di-tpyPt				FPt-thpyPt			
bond length (Å)		bond angle (deg)		bond length (Å)		bond angle (deg)	
Pt(1)–C(16)	1.975(14)	C(16)–Pt(1)–N(1)	81.3(5)	Pt(1)–C(1)	2.041(14)	C(1)–Pt(1)–N(1)	80.6(5)
Pt(2)–C(33)	1.958(14)	C(33)–Pt(2)–N(2)	81.6(6)	Pt(2)–C(22)	1.902(15)	C(22)–Pt(2)–N(2)	81.0(6)
Pt(1)–N(1)	2.001(11)	O(1)–Pt(1)–O(2)	89.7(3)	Pt(1)–N(1)	1.989(11)	O(1)–Pt(1)–O(2)	90.4(5)
Pt(2)–N(2)	1.992(13)	O(3)–Pt(2)–O(4)	89.8(4)	Pt(2)–N(2)	2.063(12)	O(3)–Pt(2)–O(4)	90.9(5)
Pt(1)–O(1)	2.073(9)			Pt(1)–O(1)	2.052(15)		
Pt(1)–O(2)	2.002(9)			Pt(1)–O(2)	1.998(14)		
Pt(2)–O(3)	2.010(10)			Pt(2)–O(3)	2.050(14)		
Pt(2)–O(4)	2.053(10)			Pt(2)–O(4)	1.997(14)		
C(3)–C(20)	1.501(16)			C(14)–C(19)	1.547(30)		

tae ligand were then reacted with 1.5 equiv of different chloromononuclear complexes and 5 equiv of Na₂CO₃ in refluxing dichloromethane for 24 h. The final products were purified by chromatography using dichloromethane and recrystallized with dichloromethane/methanol with yield at 20–30%. Synthesis of the compounds FPt(tae) and di-FPt are detailed as follows.

FPt(tae). (4',6'-dfppy)Pt(H-4',6'-dfppy)Cl (1 g, 1.64 mmol) was dissolved in 150 mL of CH₂Cl₂ followed by 2 equiv sym-tetra-acetylene (tae) (0.66 g, 3.3 mmol) and 5 equiv sodium carbonate (0.87 g, 8.2 mmol), and the solution was stirred for overnight at room temperature. The resultant slurry was filtered, and the filtrate was collected and evaporated to dryness. The product was then dissolved in small amount of dichloromethane. This solution was then chromatographed using silica-dichloromethane, where the product constituted the second fraction. The pure product was isolated as a yellow-green solid in 60% yield after recrystallization in CH₂Cl₂/MeOH.

di-FPt. (4',6'-dfppy)Pt(H-4',6'-dfppy)Cl (0.5 g, 0.82 mmol) was dissolved in 100 mL of CH₂Cl₂ followed by 0.5 equiv sym-tetra-acetylene (tae) (0.82 g, 0.41 mmol) and 5 equiv sodium carbonate (0.44 g, 4.1 mmol), and the solution was refluxed for 24 h. The purification process is similar to that of FPt(tae), except that the product was found the first fraction during chromatography. The pure product was isolated as a yellow solid in 30% yield after recrystallization in CH₂Cl₂/MeOH.

FPt(tae). Yield: 60%. ¹H NMR (360 MHz, CDCl₃), ppm: 16.72 (s, 1H), 8.95(d, 1H, *J* = 5.8 Hz), 7.98 (d, 1H, *J* = 8.2 Hz), 7.85 (t, 1H, *J* = 7.5 Hz), 7.15 (t, 1H, *J* = 6.5 Hz), 7.08 (d, 1H, *J* = 8.3 Hz), 6.58 (ddd, 1H, *J* = 12.0, 9.3, 2.4 Hz), 2.03 (s, 6H), 1.95 (s, 3H), 1.93 (s, 3H). Anal. Calcd for C₂₁H₁₉F₂NO₄Pt: C, 43.30; H, 3.29; N, 2.40. Found: C, 42.95; H, 3.30; N, 2.56.

tpyPt(tae). Yield: 45%. ¹H NMR (360 MHz, CDCl₃), ppm: 16.71 (s, 1H), 8.90 (d, 1H, *J* = 5.6 Hz), 7.76 (ddd, 1H, *J* = 9.2, 7.4, 1.8 Hz), 7.56 (d, 1H, *J* = 8.3 Hz), 7.37 (s, 1H), 7.33 (d, 1H, *J* = 7.4 Hz), 7.06 (ddd, 1H, *J* = 7.4, 5.5, 1.8 Hz), 6.91 (d, 1H, *J* = 7.4 Hz), 2.38 (s, 3H), 2.03 (s, 6H), 1.94 (s, 3H), 1.93 (s, 3H). Anal. Calcd for C₂₂H₂₃NO₄Pt: C, 47.14; H, 4.14; N, 2.50. Found: C, 47.04; H, 4.03; N, 2.63.

di-FPt. ¹H NMR (360 MHz, CDCl₃), ppm: 8.95 (d, 2H, *J* = 5.8 Hz), 7.98 (d, 2H, *J* = 8.2 Hz), 7.85 (dd, 2H, *J* = 7.5, 7.5 Hz), 7.15 (dd, 2H, *J* = 6.5, 6.5 Hz), 7.08 (d, 2H, *J* = 8.3 Hz), 6.58 (ddd, 2H, *J* = 12.0, 9.3, 2.4 Hz), 2.01 (s, 6H), 2.00 (s, 6H). Anal. Calcd for C₃₂H₂₄F₄N₂O₄Pt₂: C, 39.76; H, 2.50; N, 2.90. Found: C, 39.44; H, 2.54; N, 2.75.

Di-tpyPt. ¹H NMR (360 MHz, CDCl₃), ppm: 8.94 (d, 2H, *J* = 5.6 Hz), 7.76 (ddd, 2H, *J* = 9.2, 7.4, 1.8 Hz), 7.56 (d, 2H, *J* = 8.3 Hz), 7.41 (s, 2H), 7.34 (d, 2H, *J* = 7.4 Hz), 7.06 (ddd, 2H, *J* = 7.4, 5.5, 1.8 Hz), 6.91 (d, 2H, *J* = 7.4 Hz), 2.38 (s, 6H), 1.99 (d, 6H), 1.97 (d, 6H). Anal. Calcd for C₃₄H₃₂N₂O₄Pt₂: C, 44.25; H, 3.50; N, 3.04. Found: C, 47.2; H, 3.53; N, 2.99.

Di-thpyPt. ¹H NMR (360 MHz, CDCl₃), ppm: 8.78 (d, 2H, *J* = 5.5 Hz), 7.67 (ddd, 2H, *J* = 9.2, 7.4, 1.7 Hz), 7.49 (d, 2H,

TABLE 2: Calculated Energies for the Frontier Orbitals of the Dyads^a

dyad	HOMO–1 (eV)	HOMO (eV)	LUMO (eV)	LUMO+1 (eV)	LUMO+2 (eV)
di-FPt	–5.71	–5.70	–1.78	–1.77	–1.22
di-ppyPt	–5.41	–5.40	–1.62	–1.62	–1.06
di-thpyPt	–5.38	–5.38	–1.66	–1.66	–1.12
di-btpPt	–5.21	–5.19	–1.81	–1.81	–1.20
FPt-ppyPt	–5.64 ^b	–5.46	–1.73 ^b	–1.67	–1.14
FPt-thpyPt	–5.68 ^b	–5.40	–1.76 ^b	–1.68	–1.18
FPt-btpPt	–5.71 ^b	–5.21	–1.79	–1.78 ^b	–1.24
ppyPt-thpyPt	–5.44 ^c	–5.35	–1.65 ^c	–1.64	–1.09
ppyPt-btpPt	–5.44 ^c	–5.17	–1.76	–1.65 ^c	–1.17

^a B3LYP method with a LACVP** basis set. ^b Localized on the FPt fragment. ^c Localized on the ppyPt fragment.

J = 5.5 Hz), 7.30 (d, 2H, *J* = 8.5 Hz), 7.19 (d, 2H, *J* = 4.8 Hz), 6.90 (ddd, 2H, *J* = 7.2, 5.8, 1.4 Hz), 1.96 (s, 6H), 1.93 (s, 6H). Anal. Calcd for C₂₈H₂₄N₂O₄Pt₂S₂: C, 37.09; H, 2.67; N, 3.09. Found: C, 37.48; H, 2.57; N, 3.00.

Di-btpPt. ¹H NMR (360 MHz, CDCl₃), ppm: 8.90 (d, 2H, *J* = 6.4 Hz), 8.73–9.79 (m, 2H), 7.78–7.84 (m, 2H), 7.73 (dd, 2H, *J* = 7.4, 1.8 Hz), 7.29–7.36 (m, 6H), 6.95 (dd, 2H, *J* = 6.8, 1.5 Hz), 2.08 (s, 6H), 2.03 (s, 6H). Anal. Calcd for C₃₆H₂₈N₂O₄Pt₂S₂: C, 42.94; H, 2.80; N, 2.78. Found: C, 42.63; H, 2.74; N, 2.71.

FPt-tpyPt. ¹H NMR (360 MHz, CDCl₃), ppm: 9.00 (d, 1H, *J* = 5.6 Hz), 8.94 (d, 1H, *J* = 5.6 Hz), 7.98 (d, 1H, *J* = 8.2 Hz), 7.85 (dd, 1H, *J* = 7.5, 7.5 Hz), 7.76 (ddd, 1H, *J* = 9.2, 7.4, 1.8 Hz), 7.56 (d, 1H, *J* = 8.3 Hz), 7.41 (s, 1H), 7.34 (d, 1H, *J* = 7.4 Hz), 7.02–7.18 (m, 3H), 6.91 (d, 1H, *J* = 7.4 Hz), 6.58 (ddd, 1H, *J* = 12.0, 9.3, 2.4 Hz), 2.38 (s, 3H), 1.94–2.02 (m, 12H). Anal. Calcd for C₃₃H₂₈F₂N₂O₄Pt₂: C, 41.95; H, 2.99; N, 2.97. Found: C, 41.02; H, 2.98; N, 2.80.

FPt-thpyPt. ¹H NMR (360 MHz, CDCl₃), ppm: 9.00 (d, 1H, *J* = 5.6 Hz), 8.78 (d, 1H, *J* = 5.5 Hz), 7.98 (d, 1H, *J* = 8.2 Hz), 7.85 (t, 1H, *J* = 7.5 Hz), 7.67 (ddd, 1H, *J* = 9.2, 7.4, 1.8 Hz), 7.49 (d, 1H, *J* = 5.5 Hz), 7.30 (d, 1H, *J* = 8.5 Hz), 7.18 (d, 1H, *J* = 4.8 Hz), 7.08–7.17 (m, 2H), 6.9 (ddd, 1H, *J* = 7.2, 5.8, 1.4 Hz), 6.58 (ddd, 1H, *J* = 12.0, 9.3, 2.4 Hz), 2.0 (m, 12H). Anal. Calcd for C₃₀H₂₄F₂N₂O₄Pt₂S: C, 38.47; H, 2.58; N, 2.99. Found: C, 37.91; H, 2.48; N, 2.80.

FPt-btpPt. ¹H NMR (360 MHz, CDCl₃), ppm: 9.00 (d, 1H, *J* = 5.6 Hz), 8.9 (d, 1H, *J* = 6.4 Hz), 8.73–8.79 (m, 1H), 7.98 (d, 1H, *J* = 8.2 Hz), 7.29–7.36 (m, 3H), 7.08–7.17 (m, 2H), 6.97 (dd, 1H, *J* = 6.8, 1.5 Hz), 6.58 (ddd, 1H, *J* = 12.0, 9.3, 2.4 Hz), 2.00–2.07 (m, 12H). Anal. Calcd for C₃₄H₂₆F₂N₂O₄Pt₂S: C, 41.38; H, 2.66; N, 2.84. Found: C, 41.39; H, 2.69; N, 2.70.

tpyPt-thpyPt. ¹H NMR (360 MHz, CDCl₃), ppm: 8.94 (d, 1H, *J* = 5.6 Hz), 8.78 (d, 1H, *J* = 5.6 Hz), 7.76 (ddd, 1H, *J* = 9.2, 7.4, 1.8 Hz), 7.67 (ddd, 1H, *J* = 9.2, 7.4, 1.8 Hz), 7.56 (d,

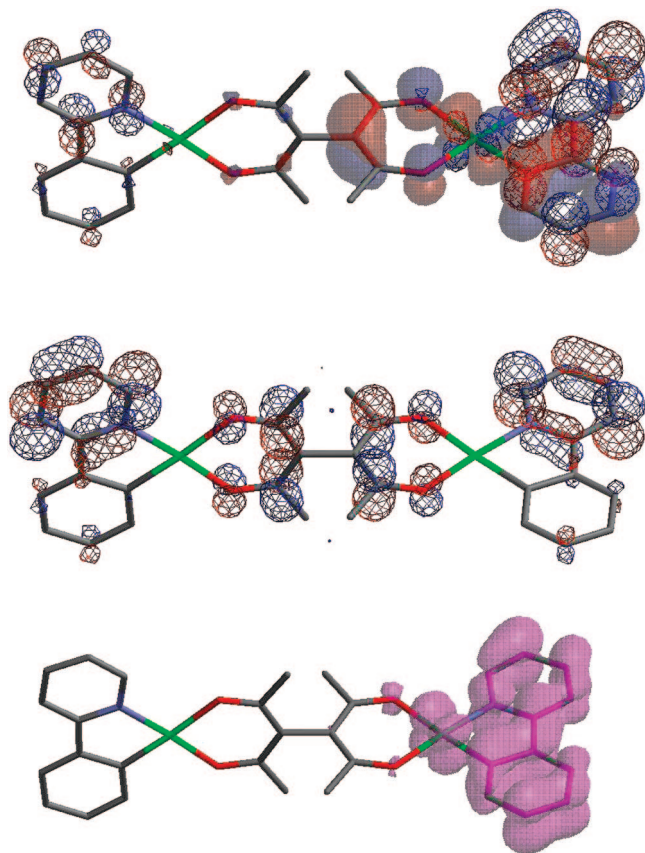


Figure 2. Molecular orbitals calculated for the di-ppyPt dyad. The HOMO (transparent) and LUMO+1 (mesh) are shown at the top. There is also a near-degenerate set of HOMO-1 and LUMO orbitals (not shown). The LUMO+2 (mesh) is shown in the middle, and the spin density (transparent) of the triplet electronic configuration is at the bottom.

1H, $J = 8.3$ Hz), 7.49 (d, 1H, $J = 5.5$ Hz), 7.41 (s, 1H), 7.28–7.36 (m, 2H), 7.19 (d, 1H, $J = 4.8$ Hz), 7.06 (dd, 1H, $J = 7.4, 5.5, 1.8$ Hz), 6.86–6.96 (m, 2H), 2.38 (s, 3H). 1.92–1.99 (m, 12H). Anal. Calcd for $C_{31}H_{28}N_2O_4Pt_2S$: C, 40.70; H, 3.09; N, 3.06. Found: C, 40.01; H, 3.01; N, 2.96.

tpyPt-bpPt. 1H NMR (360 MHz, $CDCl_3$), ppm: 8.94 (d, 1H, $J = 5.6$ Hz), 8.90 (d, 1H, $J = 6.4$ Hz), 8.73–8.79 (m, 1H), 7.68–7.83 (m, 3H), 7.56 (d, 1H, $J = 8.3$ Hz), 7.41 (s, 1H), 7.28–7.36 (m, 4H), 7.06 (ddd, 1H, $J = 7.4, 5.5, 1.8$ Hz), 6.97 (dd, 1H, $J = 6.8, 1.5$ Hz), 6.91 (d, 1H, $J = 7.4$ Hz), 2.39 (s, 3H), 1.96–2.07 (m, 12H). Anal. Calcd for $C_{35}H_{30}N_2O_4Pt_2S$: C, 43.57; H, 3.13; N, 2.90. Found: C, 43.12; H, 3.02; N, 2.95.

Results and Discussion

Syntheses and Characterization. The synthetic process used to make the dyads is similar to that used for mononuclear species reported.^{39,48} Scheme 1 shows the process used to make a series of homoleptic and heteroleptic dyads and also defines the abbreviations that will be used throughout this paper to identify the ($C^{\wedge}N$)Pt moiety. The reaction conditions were optimized in this work to obtain higher yields of the complexes. The use of dichloromethane instead of 2-ethoxyethanol as a reaction solvent increased the yield to 40–60% for mononuclear complexes compared to ~30% reported earlier. Apparently, the low boiling solvent inhibited decomposition of the metal complexes that would otherwise occur at higher temperature. Also, purification of the compounds is simplified because the reaction solvent is the same as that used for column chromatography.

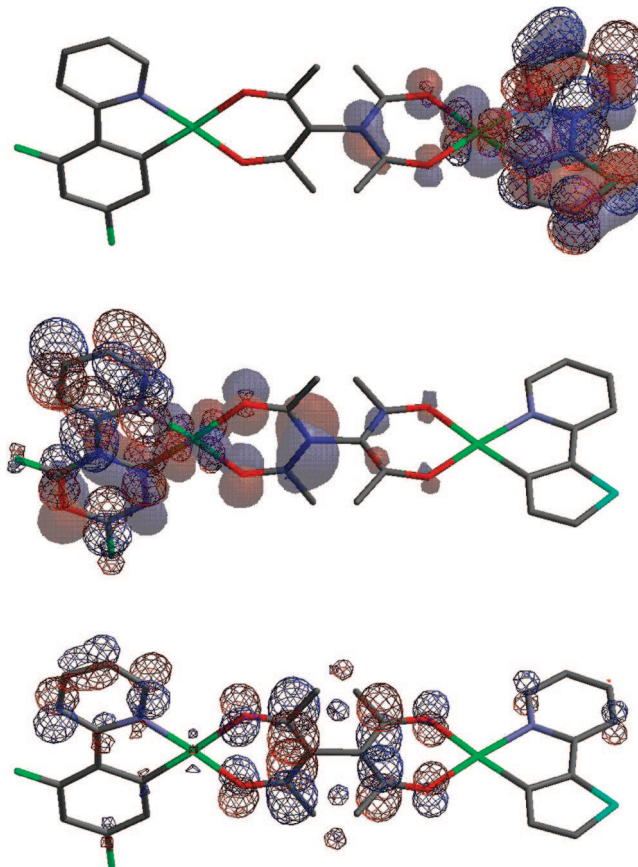


Figure 3. Molecular orbitals calculated for the FPt-thpyPt dyad. The HOMO (transparent) and LUMO+1 (mesh) are shown at the top; the HOMO-1 (transparent) and LUMO (mesh) in the middle. The LUMO+2 (mesh) is shown at the bottom.

The ratio of products obtained from these reactions depends on the stoichiometry of *tac* added to the starting mixture. To make homoleptic dyads, half-equiv of the bridging ligand *tac* was used. During this step, both homodyads and mononuclear complexes were obtained regardless of the reaction conditions. The mononuclear complexes coordinated to *tac* have an O–H bond and thus, can be easily separated and purified from the less-polar homodyad on the silica gel column, that is, dinuclear complexes in the first fraction and mononuclear complexes in the second. Isolation of the mononuclear complex provides the opportunity to coordinate a different cyclometalated Pt complex to the free diketonate ligand. Therefore, to make heteroleptic dyads, an excess of bridging ligand was used to form a mononuclear complex with *tac* and then a different cyclometalated chloro-platinum complex was added. The yields of the reactions were around 30% for homodyads and 20% for heterodyads.

The molecular formula of the obtained complexes was established using 1H NMR spectroscopy. The homodyads have the same chemical shifts as their analogous mononuclear complexes, yet the former species can be distinguished by the absence of the methine proton of the diketonate ligand. The mononuclear complexes with a *tac* ligand also display similar 1H NMR spectra as the related Pt diketonate complexes. The presence of an enolic O–H group in the singly coordinated *tac* ligand was confirmed by a proton resonance near δ 17 ppm (see the Supporting Information). For the heterodyads, the 1H NMR spectra retain the same general features exhibited by the homodyads and appear as a 1:1 superposition of the two homodyads.

X-ray Crystallographic Analysis of Di-tpyPt and FPt-thpyPt. Single crystals of a homodiyad, di-tpyPt, and a heterodiyad, FPt-thpyPt, were grown from dichloromethane/methanol solution and characterized using X-ray crystallography. The ORTEP diagrams of both complexes are shown in Figure 1; selected bond lengths and angles are listed in Table 1. For both dyads, the coordination geometry around metal centers is pseudo-square-planar with deviations from ideal planes for the C[^]N and O[^]O ligands most likely due to crystal packing forces. The metric parameters for the two halves of di-tpyPt are nearly identical to each other; values for each pair of Pt–N, Pt–O, and Pt–C bond lengths are statistically the same, as are values for the pair of C–Pt–N and O–Pt–O bond angles. The heterodiyad FPt-thpyPt has similar metric values as di-tpyPt and can be viewed as a combination of mononuclear FPt and thpyPt fragments. The nonbonding separation between Pt centers in both dyads is ca. 8.2 Å, that is, the length of the bridging ligand.

An important feature of these dyads is the molecular geometry across the tae ligand. Steric repulsion from the methyl groups of the tae ligand forces the two square-planar platinum complexes to twist such that they are nearly perpendicular to each other. The dihedral angle between planes comprising each of the three carbon atoms of the diketone units (C2–C3–C4 and C19–C20–C21 in di-tpyPt, C13–C14–C15 and C18–C19–C20 in FPt-thpyPt) are 84° in the homodiyad and 89° in the heterodiyad. A similar range of values for the twist angle (86–89°) have been reported for Co and Ru complexes that are bridged with the tae ligand.^{32–34}

DFT Calculations. Density functional theory (DFT) calculations were performed for selected dyads at the B3LYP level using a LACVP** basis set, and energies for the frontier orbitals are given in Table 2. The general picture for the electronic structure is similar for all of the homodiyads. For example, the calculated structure for di-ppyPt (ppy = 2-phenylpyridyl) has S₂ symmetry with bond lengths and angles that are within the experimental uncertainties found in the X-ray structure of the di-tpyPt complex (see the Supporting Information). The frontier molecular orbitals are shown in Figure 2 along with the spin density contour for the triplet electronic state. A near-degenerate pair of HOMO, HOMO–1 and LUMO, LUMO+1 orbitals are found to have average energies (–5.40 and –1.62 eV, respectively) that are nearly identical to the HOMO and LUMO energies determined for the mononuclear complex ppyPt(acac).³⁹ The spatial contours of the valence orbitals also conform to the pattern seen for ppyPt(acac). The HOMO is distributed among the Pt center and the phenyl and diketone moieties with a small amount delocalized on the adjacent diketone fragment. The LUMO is localized principally on the ppy ligand and the Pt center with only a minor contribution from the diketone oxygen of the tae ligand trans to carbon. The tae bridge, however, does provide a large contribution to the LUMO+2 (–1.06 eV), although there is no atomic orbital participation from the carbon atoms that connect the two diketone moieties. A single point calculation of the triplet electronic configuration leads to an energy for the ³HSOMO (–2.64 eV) that is the same as found for ppyPt(acac). The spin density contour of the triplet configuration corresponds closely to the spatial contours of the LUMO, albeit confined to a single ppyPt moiety.

A related MO structure is found for the heterodiyads. This is illustrated with the frontier orbitals for FPt-thpyPt as an example in Figure 3. The HOMO (–5.40 eV) and LUMO+1 (–1.68 eV) have the same energies and spatial contours as those calculated for the thpyPt(acac) complex. Likewise, the HOMO–1 (–5.68 eV) and LUMO (–1.76 eV) are similarly

associated with the FPt moiety, although there is some delocalization of the HOMO–1 onto the diketone portion of thpyPt fragment. The LUMO+2 (–1.18 eV) is asymmetrically disposed across the tae ligand with a greater contribution favoring the pyridyl ligand of the FPt moiety. The spin density of the triplet electronic configuration (not shown) is confined to the thpyPt fragment and has a spatial extent analogous to that seen for the di-ppyPt dyad above. The energy of the ³HSOMO (–2.50 eV) is the same as that found for the ³HSOMO of di-thpyPt. The picture that emerges from the calculations of the heterodiyads is one where the HOMO and HOMO–1 are partial delocalized across the tae bridge, whereas the LUMO and LUMO+1 are localized primarily on individual C[^]N ligands. The lowest triplet state is also localized onto a single (C[^]N)Pt moiety with minimal, if any, contribution from the tae ligand.

Electrochemistry. The electrochemical properties of the complexes were examined using cyclic voltammetry and redox data are given in Table 3. All of the electrochemical potentials reported here were measured relative to an internal ferrocenium/ferrocene (Cp₂Fe⁺/Cp₂Fe) reference. The electrochemistry of the homodiyads is similar to the mononuclear counterparts; a reversible reduction potential occurs between –2.2 and –2.40 V, whereas oxidation is irreversible. For example, di-FPt has a reversible, two-electron reduction wave at –2.31 V in DMF and an irreversible oxidation near 0.6 V as FPt (see the Supporting Information). Likewise, most of the heterodiyads show two distinct reversible, one-electron reduction waves at potentials similar to those of their respective homodiyads. For the FPt-tpyPt, FPt-thpyPt, and tpyPt-btpPt dyads, the first wave corresponds to reduction of either the FPt or btpPt moieties, whereas for the other two heterodiyads the initial site of the reduction could not be established. It is generally considered that reduction is localized on the C[^]N ligand while oxidation occurs at the metal center. The absence of any measurable separation in the reduction potentials for two reduced cyclometalated ligands of the homodiyads indicates that electronic communication through the bridging tae ligand is very weak. This behavior is consistent with the molecular orbital picture for the LUMO and LUMO+1 of di-ppyPt illustrated in Figure 2. The two unoccupied orbitals are energetically insulated from each other by the high energy LUMO+2 of the tae bridge. The tae linkage thus provides an effective energy barrier to prevent any electronic influence of a reduced C[^]N ligand from being transmitted across the bridge to the other C[^]N moiety. Unfortunately, the irreversible nature of the oxidation process precludes any meaningful analysis for the analogous effect that involves the occupied valence orbitals. However, electrochemical analysis of a [Ru(2,2'-bipyridyl)₂(tae)]²⁺ dyad shows two distinct oxidation waves separated by 90 mV,³³ which indicates that weak coupling can occur through the occupied orbitals of the tae linkage. In addition, the HOMO and HOMO–1 of di-ppyPt illustrated in Figure 2 show a large atomic orbital contribution for the carbon atoms participating in the covalent bond that links to two units together. Therefore, although the occupied orbitals are likely more effective than the unoccupied orbitals at transmitting electronic effects across the tae bridge, the magnitude of the coupling between the metal centers is probably still weak.

Absorption Spectra. UV–visible spectra were recorded for all of the complexes, and the data are given in Table 3. The absorption spectra for mononuclear tpyPt and homodiyad di-tpyPt are shown in Figure 4. The high-energy bands (<300 nm) with intense absorptivity are assigned to π–π* ligand-centered (LC) transitions. Lower-energy transitions in the range of

TABLE 3: Absorption and Redox Properties of the Complexes

complex	λ_{\max} (nm) [ϵ ($10^3 \text{ cm}^{-1} \text{ M}^{-1}$)]		$E_{1/2}$ (V) ^b
	absorption ^a		
FPt(tae)	250 (30), 275 (25), 300 (17), 319(12.8), 360 (8.4), 400sh (1.0)		-2.31
tpyPt(tae)	253 (30), 282 (28), 330 (10.6), 360 (7.9), 400sh (2)		-2.39
di-FPt	251 (55), 275 (34), 307 (20), 321 (21), 365 (16.8), 400sh (2.1)		-2.31
di-tpyPt	255 (53), 282 (40), 316 (21), 330 (19), 366 (16), 400 (6.5), 420sh (1.5)		-2.37
di-thpyPt	292 (32), 317 (30), 334 (32), 364 (19), 402 (10.8), 423 (9.2)		-2.31
di-btpPt	265 (38), 277 (36), 286 (35), 318 (37), 346 (28), 372 (17), 426 (15), 445 (14)		-2.25
FPt-tpyPt	250 (62), 277 (37), 307 (22), 321 (22), 370 (17), 400sh (6.0)		-2.27, -2.37
FPt-thpyPt	251 (44), 276 (30), 310 (24), 320 (25), 335 (22), 360 (18), 423 (4.6)		-2.30, -2.38
FPt-btpPt	248 (46), 274 (34), 309 (25), 320 (28), 348 (20), 368 (17), 424 (6.5), 446 (6.3)		-2.27
tpyPt-thpyPt	253 (41), 285 (36), 318 (27), 333 (27), 365 (18), 402 (8.9), 425 (5.5)		-2.31, -2.37
tpyPt-btpPt	254 (46), 282 (38), 318 (29), 348 (22), 372 (16), 422 (7.6), 446 (6.8)		-2.26, -2.50

^a Absorption measurements were carried out in CH_2Cl_2 . ^b Redox measurements were carried out in DMF solution; values are reported relative to $\text{Cp}_2\text{Fe}^+/\text{Cp}_2\text{Fe}$.

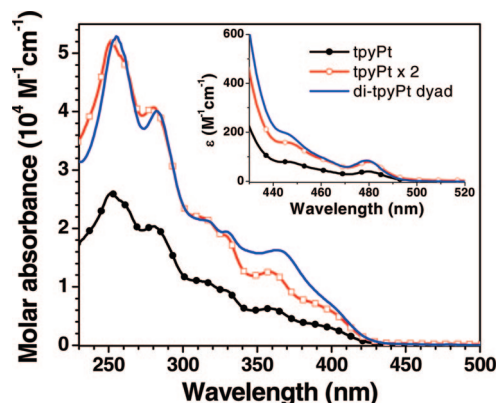


Figure 4. Absorption spectra for tpyPt and di-tpyPt; the inset shows the lowest energy absorption features. The spectra were measured in dichloromethane at room temperature.

350–450 nm are assigned as metal-to-ligand charge-transfer (MLCT) transitions. Figure 4 also shows the curve of a twofold mathematical sum of the molar absorbance for the mononuclear tpyPt(acac) complex. The dyad spectrum conforms to that of the summed spectrum in the high-energy transition range above 300 nm, whereas the intensity increases in the region of the MLCT transitions near 360 nm and is accompanied by a small red-shift of 5 nm. Similar spectral characteristics are found in the other platinum dyads (see the Supporting Information). The changes in the MLCT region of the dyad are tentatively assigned to an intramolecular charge-transfer transition(s) from the lowest occupied orbitals to the LUMO+2 that is delocalized across the tae bridging ligand. Close examination of the lowest excited state (inset of Figure 4) shows that the singlet-to-triplet transition for the dyad is at the same wavelength and nearly twice the intensity as that of the mononuclear species. Because DFT calculations show little to no interaction between the degenerate frontier MO's of the homodyad, it is not surprising that the extinction coefficient is roughly twice that of the mononuclear complex. It is apparent from the absorption spectrum that the energy of the T_1 state, which is determined mainly by the nature of the cyclometalating ligand, is minimally affected by the bridging tae ligand.

The absorption spectra for the heterodyad FPt-thpyPt along with the di-FPt and di-thpyPt homodyads are shown in Figure 5; spectra for the other heterodyads are given in the Supporting Information. The absorption spectrum of the FPt-thpyPt complex

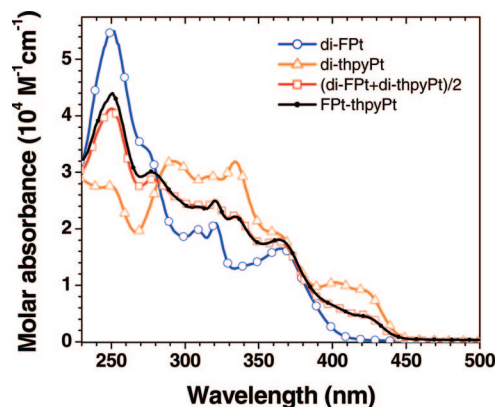


Figure 5. Absorption spectra of di-FPt, di-thpyPt, and heterodyad FPt-thpyPt. The spectra were measured in dichloromethane at room temperature.

is almost identical to the one created by a simple arithmetic average of the spectra for the two homodyads. No new features are observed, which indicates that the two different cyclometalated moieties act as two independent chromophores with little to no ground-state electronic interaction between them.

Emission and Energy Transfer. Homodyads. All of the homodyads are intensely emissive in low-temperature glasses (77 K) and in fluid solution at 298 K. The emission properties of the compounds at 77 K are listed in the Table 4. For homodyads, the emission spectra are indistinguishable from their mononuclear counterparts. Figure 6 displays the excitation and emission spectra of di-tpyPt and tpyPt(acac) at 77 K; the inset shows the emission at room temperature. The pronounced vibronic features in the luminescence spectra, along with microsecond lifetimes for emission decay, indicate phosphorescence that originates from a mixed $^3\text{LC-MLCT}$ triplet state on the cyclometalated ligand. Because the bridging tae ligand does not alter the triplet energy of the (C^{N})Pt moiety, the emission energy of the homodyads can be varied easily by appropriate choice of the C^{N} ligand (Figure 7) in a manner similar to that reported for their mononuclear analogs.³⁹

Although the bridging tae ligand does not affect the emission energy, other properties, such as luminescent decay rates, are altered upon formation of the homodyad. The emission lifetimes of di-FPt and di-tpyPt are ca. 20% shorter than their mononuclear counterparts. For the di-thpyPt and di-btpPt complexes, the lifetimes for dyads and corresponding mononuclear com-

TABLE 4: Emission Properties and Intramolecular Energy Transfer Rates for Dyads

complex	emission at 77K ^a				
	high-energy complex in dyad		low-energy complex in dyad		energy transfer rate (s ⁻¹) and transfer efficiency
	λ_{\max} , nm	τ , μ s ^b	λ_{\max} , nm	τ , μ s	
di-FPt	458	6.5 (8.1)			
di-tpyPt	480	8.4 (10.2)			
di-thpyPt	550	17.7 (17.7)			
di-btpPt	598	10.4 (10.5)			
FPt-tpyPt	458	0.1	480	8.4	9.9×10^6 (98.5%)
FPt-thpyPt	458	0.01	550	18.4	1.0×10^8 (99.8%)
FPt-btpPt	458	0.08	598	10.5	1.2×10^7 (98.8%)
tpyPt-thpyPt	480	0.07	550	17.2	1.4×10^7 (99.2%)
tpyPt-btpPt	480	0.07	598	10.3	1.4×10^7 (99.2%)

^a Emission and lifetime measurements were carried out in 2-MeTHF. ^b Lifetimes for homodyads are listed along with lifetimes for their mononuclear analogs in parentheses.

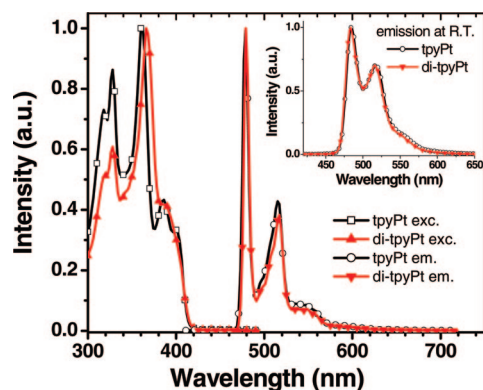


Figure 6. Emission and excitation for di-tpyPt and tpyPt at 77 K in 2-MeTHF; the inset is the emission spectra in fluid solution at 298 K.

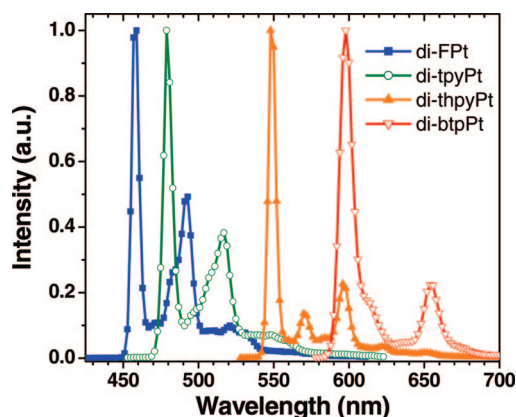


Figure 7. Emission spectra of homodyads at 77 K in 2-MeTHF glass.

plexes are the same. A priori, the lifetimes for di-FPt and di-tpyPt could be shortened by an increase in either the nonradiative (k_{nr}) or radiative (k_r) decay rate. Radiationless decay of luminescent transition-metal complexes at 77 K occurs primarily through vibronic coupling of the lowest ³MLCT state with the ground state.^{50,51} The close similarity in the emission line shapes of the dyads with their mononuclear analogs indicates that common vibrational modes are present in both types of complexes and, thus, the k_{nr} values should be similar among them as well. Therefore, an increase in k_r is most likely the origin for the shorter lifetimes of the dyads. A higher value of k_r could arise from two effects: an increase in the oscillator strength of the singlet state that is coupled to the luminescent triplet state and/or a decrease in the energy separation between

the two states.^{52,53} The absorption spectra of the dyads show an increase in the molar absorptivity of the MLCT bands near 365 nm that can implement the first effect. In addition, the same absorption transitions are red-shifted relative to the mononuclear complexes such that the decrease in the singlet–triplet gap can also contribute to the rise in the radiative decay rate. For di-thpyPt and di-btpPt, however, these perturbations are ineffectual because the large energy separation between the interacting states ($9000\text{--}10500\text{ cm}^{-1}$) greatly attenuates the coupling effects.

Another notable difference in emissive behavior occurs between di-FPt and its mononuclear analog, FPt(acac), in fluid solution. A common characteristic of luminescent square-planar Pt complexes is a strong propensity to undergo self-quenching in fluid solution via the formation of excimers.⁵⁴ Platinum complexes with cyclometalated 2-(4,6-difluorophenyl)pyridyl ligands, such as FPt(acac), are exemplary in this regard in that their emission lifetimes in 2-MeTHF are shortened to $<1\ \mu\text{s}$ at room temperature.^{39,55} Likewise, the di-FPt dyad undergoes efficient self-quenching under the same conditions. A plot of the lifetime versus concentration for the di-FPt complex yields a linear correlation (see the Supporting Information). The intrinsic lifetime of di-FPt was determined to be 250 ns from the intercept of the lifetime versus concentration plot, while the corresponding value for FPt(acac) is 330 ns. The second-order rate constant for self-quenching of di-FPt ($1.9 \times 10^9\ \text{M}^{-1}\text{s}^{-1}$) is only half that of FPt(acac) ($4.0 \times 10^9\ \text{M}^{-1}\text{s}^{-1}$). The luminescent spectra of di-FPt, however, show a significant difference with that of FPt(acac). Figure 8 displays the emission spectra of di-FPt at two different concentrations ($1.0 \times 10^{-5}\ \text{M}$ and $5.0 \times 10^{-2}\ \text{M}$) in 2-MeTHF, along with luminescence from FPt at a concentration of $1.5 \times 10^{-2}\ \text{M}$. Self-quenching of the mononuclear FPt(acac) complex occurs with a concomitant growth in a broad, featureless emission at low energy ($>600\ \text{nm}$), whereas low-energy luminescence from concentrated solutions of di-FPt is largely suppressed. The transient emission decay at both short and long wavelengths from a concentrated solution of di-FPt is shown in the inset of Figure 8. Analysis of the initial rise time of the transient decay curve gives an estimated lifetime for the low-energy emission of 90 ns; the corresponding value for FPt(acac) is 135 ns. The close similarity in self-quenching kinetics between di-FPt and FPt(acac) suggests a common origin for the deactivating state despite the difference in luminescent spectra. The broad, structureless luminescence from FPt(acac) is believed to arise from an excimer with a close Pt \cdots Pt interaction.⁵⁶ Luminescent dimers with related $d^8\cdots d^8$ interactions are ubiquitous in solid-state structures of square-planar Pt complexes.^{57,58} The low-energy transitions occur when

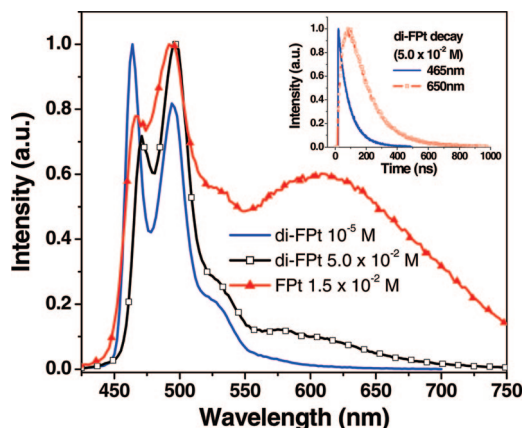


Figure 8. Emission spectra of di-FPt and FPt at different concentrations in 2-MeTHF solution at 298 K; the inset shows the transient decay at two different wavelengths for di-FPt at high concentration.

the Pt centers approach to within 3.5 Å of each other and destabilize the HOMO through overlap of filled valence d_{z^2} orbitals. The absence for such an emission feature from concentrated solutions of the di-FPt complex can be attributed to steric shielding from the *tae* ligand. Computer modeling of di-FPt indicates that the pair of methyl groups of the *tae* ligand that protrude above the adjacent Pt square plane prevent any close intermolecular Pt \cdots Pt contact (<4 Å) with a Pt center from a second dyad. Therefore, the efficient self-quenching in di-FPt cannot be ascribed to deactivation caused by Pt \cdots Pt interactions and instead is most likely brought about by nonradiative decay that involves π – π contacts.

Heterodyads. The presence of two different lumiphores in the heterodyads enables the study of intramolecular triplet energy transfer process across the *tae* bridging ligand. To avoid complications due to intermolecular energy transfer from the long-lived triplet state, the emission characteristics of the heterodyads were examined using dilute solutions (<10⁻⁵ M) in rigid 2-MeTHF glass at 77 K. An example of the excitation and emission spectra from the FPt-thyPt dyad, along with spectra from the corresponding homodyads, is shown in Figure 9. Spectra of the other heterodyads are given in the Supporting Information. All of the heterodyads display dual luminescence. Emission comes principally from the low-energy Pt species while much weaker luminescence is observed from the higher-energy fragment of the heterodyad. The high- and low-energy transitions have spectra that are identical to those of the homodyads, suggesting that the two (C \wedge N)Pt moieties act as independent lumiphores. The residual emission from the higher-energy donor enables the intramolecular energy-transfer rate to be calculated from the transient decay using the equation $K_{ET} = 1/\tau - 1/\tau_0$, where τ is the lifetime of the donor in presence of the acceptor and τ_0 is the lifetime of the donor alone. The efficiency of energy transfer can also be determined using $\Phi_{ET} = 1 - \tau/\tau_0$. The results of these calculations are listed in Table 4. It is apparent that rapid triplet transfer from the high-energy donor across the bridging ligand is still possible despite the orthogonal disposition of the *tae* linkage.

Triplet energy can undergo nonradiative transfer between the two halves of the dyad by two basic processes, dipole–dipole (Förster) or electron exchange (Dexter). Förster energy transfer involves resonant, through-space interactions and is typically employed to describe transfer between singlet states, whereas the latter process relies on orbital overlap and is more often associated with transfer involving triplet states. Nonetheless, resonant Förster transfer between triplet states has been dem-

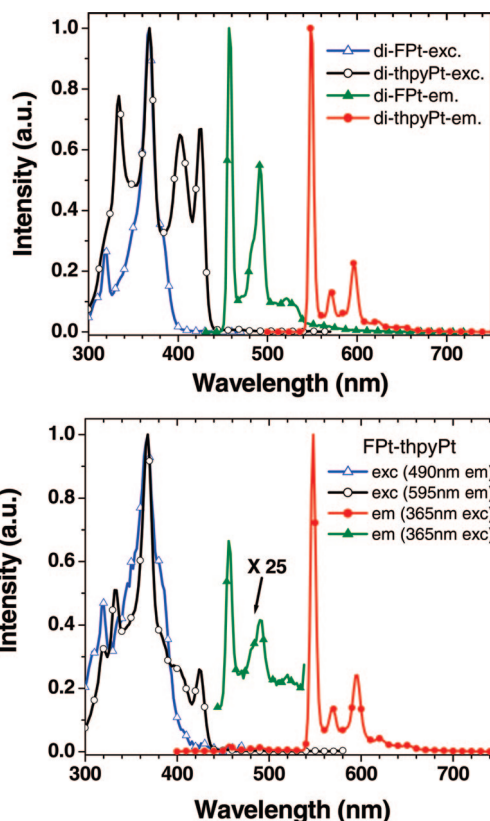


Figure 9. Excitation and emission spectra for thyPt with FPt emission spectra at 77 K (top) and FPt-thyPt dyad excitation and emission spectra (bottom). The enhanced emission spectrum from the FPt moiety in the heterodyad is offset for clarity.

onstrated to occur between cyclometalated Ir complexes.⁵⁹ The rate of energy transfer from either mechanism is proportional to the spectral overlap (J) between the donor emission and acceptor absorption spectra. For Förster transfer, the rate equation takes the form

$$k_f = \frac{8.8 \times 10^{-25} K^2 \Phi_D J_F}{n^4 \tau_D r^6} \quad (1)$$

where K is an orientation factor for the interacting dipoles, Φ_D is the luminescent quantum yield of the donor, n is the refractive index of the solvent (1.405 for 2-MeTHF), τ_D is the lifetime of the donor, r is the donor–acceptor distance, and J_F is spectral overlap integral, which incorporates the molar absorbance of the acceptor. The triplet character of the lowest-energy absorption bands (>450 nm) in the thyPt moiety leads to weak absorptivity for these transitions, similar to values shown for di-tyPt in Figure 4, and therefore the spectra overlap with the FPt emission is poor. For FPt-thyPt, $J_F \approx 1.0 \times 10^{-15} \text{ cm}^6 \text{ mmol}^{-1}$ and, thus, assuming $K^2 = 2/3$ (for random transition dipoles) and $\Phi_D = 1$, the Förster radius (r_0 , the distance where $k_f = 1/\tau_D$) for this system is ca. 22 Å. However, Förster transfer is strongly dependent on the angular orientation of the interacting dipole moments. Because the *tae* ligand of FPt-thyPt imposes an orthogonal arrangement on the two (C \wedge N)Pt fragments, the value of K^2 will approach zero and consequently decrease r_0 to less than 10 Å; that is, the separation distance between the cyclometalated ligands. Therefore, resonant transfer should be only a minor component to the energy-transfer process in this system.

Simple Dexter transfer between triplet states, although dominant at short distances (<10 Å), is problematic in these

dyad complexes. The electron exchange process requires that there be good overlap between the molecular orbitals involved in the donor and acceptor triplet states. However, the phosphorescent spectra and DFT calculations of the spin density for these systems indicate that the triplets are insulated from each other and restricted to orbitals on the (C[^]N)Pt portions of the dyads. Triplet energy transfer in this case resembles the situation found in donor–bridge–acceptor (D–B–A) molecules.⁶⁰ In such D–B–A systems, triplet transfer is viewed as the product of a pair of hole- and electron-transfer events that utilize the HOMO and LUMO, respectively, of the bridging ligand to facilitate charge transfer.⁶¹ Charge can move either by an incoherent hopping process that involves oxidizing and/or reducing the bridge or by a superexchange process that involves virtual excitations of the bridging moiety.⁶² Hopping is favored when the energy separation between the donor and bridge are within several *kT* of each other; otherwise, the latter process is invoked. The energetic and spatial picture for the MOs of the heterodyads suggests that a combination of both hopping and superexchange mechanisms could be involved in the energy-transfer process. On the basis of the DFT calculations, hole transfer is either exergonic for heterodyads that have an FPt moiety or energetically neutral for those with a tpyPt donor. The spatial delocalization of the HOMOs associated with these donors onto the HOMOs of the acceptors as shown in Figures 2 and 3 should allow enough orbital overlap to facilitate the direct hop of a hole across the *tae* ligand. Alternatively, electron transfer can be endergonic (FPt-tpyPt and FPt-thpyPt), neutral (FPt-btpPt and tpyPt-thpyPt), or exergonic (tpyPt-btpPt), yet there is no apparent correlation with the driving force on the energy-transfer rate. Moreover, the absence of any signature for interactions between anion states in the $E_{1/2}^{\text{red}}$ values or LUMO and LUMO+1 energies determined from DFT calculations indicates that there is no direct orbital pathway available for an electron to hop across the *tae* linkage. In this case, a superexchange mechanism that is mediated by the LUMO+2 provides a viable route for electrons to traverse the bridge.⁶³ In superexchange theory, the rate of electron transfer is proportional to the square of the coupling between the donor and acceptor (V_{DA}) according to the approximate expression $V_{DA} = V_{DB} \times V_{BA}/\Delta E_{DB}$, where V_{DB} and V_{BA} are the electronic couplings between the donor–bridge and bridge–acceptor, respectively, and ΔE_{DB} is the energy gap between the donor–bridge.⁶⁴ An estimate for the value of ΔE_{DB} (0.60 eV) can be obtained from the calculated values for the LUMOs of either FPt or tpyPt donor the LUMO+2 bridge (Table 2). The other heterodyads have comparable values for ΔE_{DB} (0.50–0.60 eV). Therefore, if one assumes a relatively constant value for $V_{DB} \times V_{BA}$ due to the identical nature of the pyridyl donors and acceptors in the other heterodyads, then the rate of electron (and likewise, energy) transfer should also be similar for these complexes, as is found to be the case here.

Conclusions

In summary, the cyclometalated Pt dyads presented in this work appear, at first glance, to have electronic properties expected for two covalently linked, independent chromophores. The electrochemical characteristics and emission energies of the homodyads are identical to those of their mononuclear analogs. However, the presence of the *tae* ligand does appear to increase the radiative rate of di-FPt and di-tpyPt relative to the mononuclear derivatives. In addition, although the steric bulk of the *tae* ligand does little to inhibit self-quenching of di-FPt in fluid solution, luminescence from excimeric species with

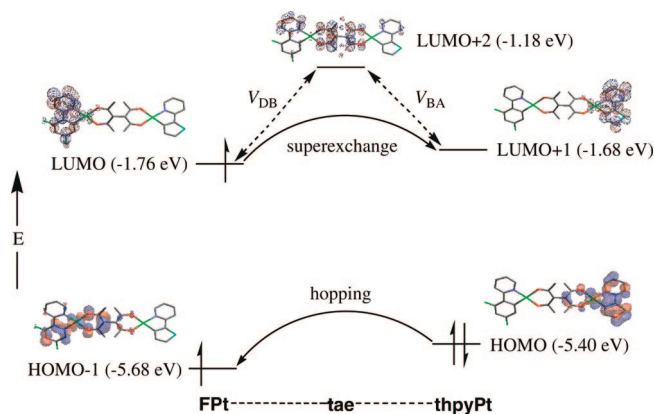


Figure 10. Schematic energy-level diagram showing the different pathways proposed for charge transfer in FPt-thpyPt.

Pt^{•••}Pt interactions is suppressed. Otherwise, the luminescent properties of the cyclometalated Pt moieties in the homodyads are unaltered by the bridging ligand. These characteristics are useful in deciphering specific orbital features responsible for the efficient energy transfer that takes place in the heterodyads. The orthogonal geometric orientation between the Pt units allows us to treat Förster processes as negligible and focus on the key orbitals that are involved in Dexter-like triplet transfer. Delocalization within the occupied valence orbitals of the *tae* ligand should enable facile hole transfer, whereas electron transfer will be governed by the electronic coupling between unoccupied orbitals on the *tae* ligand and the LUMOs localized on the (C[^]N)Pt moieties. This picture of distinct orbital pathways for the hole- and electron-exchange mechanism that dictates triplet transfer suggests a means to systematically modify the energy-transfer rate through appropriate synthetic modification of the bridging ligand. One possibility would be to replace the single covalent bond between the diketonate ligands of the *tae* linkage with phenylene spacers.⁶⁵ Another option would be to use a different type of bridging ligand, such as tetra-pyrazolylborates,⁶⁶ that maintain the same essential geometric features as *tae*, but change the identity of the ligand coordinated to the metal centers. Work is underway in our laboratories to explore some of these potential synthetic routes in order to alter the rate of triplet transfer that occurs between the cyclometalated units.

Acknowledgment. We thank Jonas Oxgaard (California Institute of Technology) for helpful discussions regarding the theoretical calculations. We also thank Universal Display Corporation for support of this work.

Supporting Information Available: ¹H NMR spectra of tpyPt(*tae*), di-tpyPt, and tpyPt(*acac*); cyclic voltammetric traces for di-FPt and FPt(*acac*); selected bond lengths and angles for di-tpyPt and FPt-thpyPt obtained from DFT calculations; molecular orbital diagrams from DFT calculations for the dyads; absorption and emission spectra of dyads; crystallographic data and CIF files for di-tpyPt and FPt-thpyPt. This information is available free of charge via the Internet at <http://pubs.acs.org>.

References and Notes

- Balzani, V.; Juris, A.; Venturi, M.; Campagna, S.; Serroni, S. *Chem. Rev.* **1996**, *96*, 759.
- Hissler, M.; McGarrah, J. E.; Connick, W. B.; Geiger, D. K.; Cummings, S. D.; Eisenberg, R. *Coord. Chem. Rev.* **2000**, *208*, 115.
- Sun, S. S.; Lees, A. J. *Coord. Chem. Rev.* **2002**, *230*, 171.
- Welter, S.; Brunner, K.; Hofstraat, J. W.; De Cola, L. *Nature* **2003**, *421*, 54.

- (5) Chiorboli, C.; Indelli, M. T.; Scandola, F. *Top. Curr. Chem.* **2005**, 257, 63.
- (6) Ceccon, A.; Santi, S.; Orian, L.; Bisello, A. *Coord. Chem. Rev.* **2004**, 248, 683.
- (7) Balzani, V.; Juris, A. *Coord. Chem. Rev.* **2001**, 211, 97.
- (8) Barigelletti, F.; Flamigni, L. *Chem. Soc. Rev.* **2000**, 29, 1.
- (9) De Cola, L.; Belser, P. *Coord. Chem. Rev.* **1998**, 177, 301.
- (10) Wasielewski, M. R. *Chem. Rev.* **1992**, 92, 435.
- (11) Speiser, S. *Chem. Rev.* **1996**, 96, 1953.
- (12) Willner, I.; Kaganer, E.; Joselevich, E.; Durr, H.; David, E.; Gunter, M. J.; Johnston, M. R. *Coord. Chem. Rev.* **1998**, 171, 261.
- (13) Collin, J. P.; Guillerez, S.; Sauvage, J. P.; Barigelletti, F.; Decola, L.; Flamigni, L.; Balzani, V. *Inorg. Chem.* **1991**, 30, 4230.
- (14) Amouyal, E.; Mouallembahout, M. *J. Chem. Soc., Dalton Trans.* **1992**, 509.
- (15) Collin, J. P.; Guillerez, S.; Sauvage, J. P.; Barigelletti, F.; Decola, L.; Flamigni, L.; Balzani, V. *Inorg. Chem.* **1992**, 31, 4112.
- (16) Flamigni, L.; Armaroli, N.; Barigelletti, F.; Balzani, V.; Collin, J. P.; Dalbavie, J. O.; Heitz, V.; Sauvage, J. P. *J. Phys. Chem. B* **1997**, 101, 5936.
- (17) Indelli, M. T.; Scandola, F.; Flamigni, L.; Collin, J. P.; Sauvage, J. P.; Sour, A. *Inorg. Chem.* **1997**, 36, 4247.
- (18) Lee, J. D.; Vrana, L. M.; Bullock, E. R.; Brewer, K. J. *Inorg. Chem.* **1998**, 37, 3575.
- (19) Hissler, M.; Harriman, A.; Khatyr, A.; Ziessel, R. *Chem.—Eur. J.* **1999**, 5, 3366.
- (20) Dixon, I. M.; Collin, J. P.; Sauvage, J. P.; Flamigni, L. *Inorg. Chem.* **2001**, 40, 5507.
- (21) Ceroni, P.; Laghi, I.; Maestri, M.; Balzani, V.; Gestermann, S.; Gorka, M.; Vogtle, F. *New J. Chem.* **2002**, 26, 66.
- (22) Chiorboli, C.; Rodgers, M. A. J.; Scandola, F. *J. Am. Chem. Soc.* **2003**, 125, 483.
- (23) McGarrah, J. E.; Eisenberg, R. *Inorg. Chem.* **2003**, 42, 4355.
- (24) Baranoff, E.; Dixon, I. M.; Collin, J. P.; Sauvage, J. P.; Ventura, B.; Flamigni, L. *Inorg. Chem.* **2004**, 43, 3057.
- (25) Thomas, K. R. J.; Lin, J. T.; Tao, Y. T.; Chuen, C. H. *Chem. Mater.* **2004**, 16, 5437.
- (26) Wadas, T. J.; Chakraborty, S.; Lachicotte, R. J.; Wang, Q. M.; Eisenberg, R. *Inorg. Chem.* **2005**, 44, 2628.
- (27) Bettington, S.; Tavasli, M.; Bryce, M. R.; Batsanov, A. S.; Thompson, A. L.; Al Attar, H. A.; Dias, F. B.; Monkman, A. P. *J. Mater. Chem.* **2006**, 16, 1046.
- (28) Laine, P. P.; Bedioui, F.; Loiseau, F.; Chiorboli, C.; Campagna, S. *J. Am. Chem. Soc.* **2006**, 128, 7510.
- (29) Förster, T. *Discuss. Faraday Soc.* **1959**, 7.
- (30) Dexter, D. L. *J. Chem. Phys.* **1953**, 21, 836.
- (31) Faure, S.; Stern, C.; Guillard, R.; Harvey, P. D. *J. Am. Chem. Soc.* **2004**, 126, 1253.
- (32) Zhang, Y.; Wang, S.; Enright, G. D.; Breeze, S. R. *J. Am. Chem. Soc.* **1998**, 120, 9398.
- (33) Koiwa, T.; Masuda, Y.; Shono, J.; Kawamoto, Y.; Hoshino, Y.; Hashimoto, T.; Natarajan, K.; Shimizu, K. *Inorg. Chem.* **2004**, 43, 6215.
- (34) Zhang, Y. S.; Breeze, S. R.; Wang, S. N.; Greedan, J. E.; Raju, N. P.; Li, L. J. *Can. J. Chem.—Revue Canadienne De Chimie* **1999**, 77, 1424.
- (35) Newton, M. D. *Coord. Chem. Rev.* **2003**, 238, 167.
- (36) Lamansky, S.; Djurovich, P.; Murphy, D.; Abdel-Razzaq, F.; Kwong, R.; Tsyba, I.; Bortz, M.; Mui, B.; Bau, R.; Thompson, M. E. *Inorg. Chem.* **2001**, 40, 1704.
- (37) Lamansky, S.; Djurovich, P.; Murphy, D.; Abdel-Razzaq, F.; Lee, H. E.; Adachi, C.; Burrows, P. E.; Forrest, S. R.; Thompson, M. E. *J. Am. Chem. Soc.* **2001**, 123, 4304.
- (38) Adamovich, V.; Brooks, J.; Tamayo, A.; Alexander, A. M.; Djurovich, P. I.; D'Andrade, B. W.; Adachi, C.; Forrest, S. R.; Thompson, M. E. *New J. Chem.* **2002**, 26, 1171.
- (39) Brooks, J.; Babayan, Y.; Lamansky, S.; Djurovich, P. I.; Tsyba, I.; Bau, R.; Thompson, M. E. *Inorg. Chem.* **2002**, 41, 3055.
- (40) *Highly Efficient OLEDs with Phosphorescent Materials*; Yersin, H., Ed.; Wiley-VCH: Berlin, 2007.
- (41) Sabatini, C.; Barbieri, A.; Barigelletti, F.; Arm, K. J.; Williams, J. A. G. *Photochem. Photobiol. Sci.* **2007**, 6, 397.
- (42) Auffranch, A.; Barbieri, A.; Barigelletti, F.; Lacour, J.; Mobian, P.; Collin, J. P.; Sauvage, J. P.; Ventura, B. *Inorg. Chem.* **2007**, 46, 6911.
- (43) Auffranch, A.; Barbieri, A.; Barigelletti, F.; Collin, J. P.; Flamigni, L.; Sabatini, C.; Sauvage, J. P. *Inorg. Chem.* **2006**, 45, 10990.
- (44) Welter, S.; Lafolet, F.; Cecchetto, E.; Vergeer, F.; De Cola, L. *ChemPhysChem* **2005**, 6, 2417.
- (45) Lafolet, F.; Welter, S.; Popovic, Z.; De Cola, L. *J. Mater. Chem.* **2005**, 15, 2820.
- (46) Plummer, E. A.; Hofstraat, J. W.; De Cola, L. *Dalton Trans.* **2003**, 2080.
- (47) Du, H.; Fuh, R. C. A.; Li, J. Z.; Corkan, L. A.; Lindsey, J. S. *Photochem. Photobiol.* **1998**, 68, 141.
- (48) Cho, J. Y.; Suponitsky, K. Y.; Li, J.; Tirnofeeva, T. V.; Barlow, S.; Marder, S. R. *J. Organomet. Chem.* **2005**, 690, 4090.
- (49) Cockburn, B. N.; Howe, D. V.; Keating, T.; Johnson, B. F. G.; Lewis, J. J. *Chem. Soc., Dalton Trans.* **1973**, 404.
- (50) Kober, E. M.; Caspar, J. V.; Lumpkin, R. S.; Meyer, T. J. *J. Phys. Chem.* **1986**, 90, 3722.
- (51) Caspar, J. V.; Meyer, T. J. *J. Phys. Chem.* **1983**, 87, 952.
- (52) Li, J.; Djurovich, P. I.; Alleyne, B. D.; Yousufuddin, M.; Ho, N. N.; Thomas, J. C.; Peters, J. C.; Bau, R.; Thompson, M. E. *Inorg. Chem.* **2005**, 44, 1713.
- (53) Vanhelmont, F. W. M.; Güdel, H. U.; Förtsch, M.; Bürgi, H. B. *Inorg. Chem.* **1997**, 36, 5512.
- (54) Fleeman, W. L.; Connick, W. B. *Comments Inorg. Chem.* **2002**, 23, 205.
- (55) Ma, B. W.; Djurovich, P. I.; Thompson, M. E. *Coord. Chem. Rev.* **2005**, 249, 1501.
- (56) Ma, B. W.; Djurovich, P. I.; Garon, S.; Alleyne, B.; Thompson, M. E. *Adv. Funct. Mater.* **2006**, 16, 2438.
- (57) Connick, W. B.; Marsh, R. E.; Schaefer, W. P.; Gray, H. B. *Inorg. Chem.* **1997**, 36, 913.
- (58) Houlding, V. H.; Miskowski, V. M. *Coord. Chem. Rev.* **1991**, 111, 145.
- (59) Wasserberg, D.; Meskers, S. C. J.; Janssen, R. A. J. *J. Phys. Chem. A* **2007**, 111, 1381.
- (60) Albinsson, B.; Eng, M. P.; Pettersson, K.; Winters, M. U. *Phys. Chem. Chem. Phys.* **2007**, 9, 5847.
- (61) Closs, G. L.; Piotrowiak, P.; Macinnis, J. M.; Fleming, G. R. *J. Am. Chem. Soc.* **1988**, 110, 2652.
- (62) Weiss, E. A.; Wasielewski, M. R.; Ratner, M. A. *Top. Curr. Chem.* **2005**, 257, 103.
- (63) McConnell, H. M. *J. Chem. Phys.* **1961**, 35, 508.
- (64) Paulson, B. P.; Miller, J. R.; Gan, W. X.; Closs, G. J. *Am. Chem. Soc.* **2005**, 127, 4860.
- (65) Lambert, J. B.; Liu, Z. Q. *J. Chem. Crystallography* **2007**, 37, 629.
- (66) Li, J.; Djurovich, P. I.; Alleyne, B. D.; Tsyba, I.; Ho, N. N.; Bau, R.; Thompson, M. E. *Polyhedron* **2004**, 23, 419.